Earth, Planets and Space

FULL PAPER Open Access

Not trench-parallel but trench-normal source fault of the 1994 Hokkaido Toho-oki earthquake as revealed by the aftershock relocation using HypoDD

Kei Katsumata[1*]

Abstract

In the southwestern area of the Kurile Islands subduction zone, three large earthquakes including the M_w8.2 1969 and the M_w8.3 1994 Hokkaido Toho-oki earthquakes and the M_w7.8 1975 tsunami earthquake occurred in almost the same location. The three main shocks and their aftershocks were re-determined simultaneously using a double-difference earthquake location method, HypoDD. As a result, the 1969 and the 1975 main shocks and their aftershocks were concentrated near the upper surface of the subducting Pacific plate, indicating that both events were plate boundary megathrust earthquakes as shown by previous studies. On the other hand, the 1994 main shock and its aftershocks were distributed within the Pacific plate indicating that the 1994 event was an intraslab event as reported by previous studies. The result that interplate earthquakes and intraslab earthquakes could be appropriately distinguished is strong evidence that the accuracy of hypocenter determination is sufficiently high. The centroid moment tensor solution of the 1994 main shock has two nodal planes which are parallel or normal to the Kurile Trench. According to the high-resolution hypocenter distribution obtained in the present study, the aftershocks appear to locate on the nodal plane normal to the trench, suggesting that the source fault ruptured by the 1994 main shock was not parallel but normal to the Kurile Trench. Moreover, we found that the Coulomb failure stress change (ΔCFS) produced by the trench-normal fault plane is more likely to trigger the largest aftershock than ΔCFS produced by the trench-parallel fault plane.

Keywords Aftershock distribution, HypoDD, Kurile Islands, The Hokkaido-Toho-oki earthquakes, Coulomb failure stress change

This is a manuscript for the special issue "New trends in data acquisition, analysis and interpretation of seismicity".

*Correspondence:
Kei Katsumata
kkatsu@sci.hokudai.ac.jp

Graphical abstract

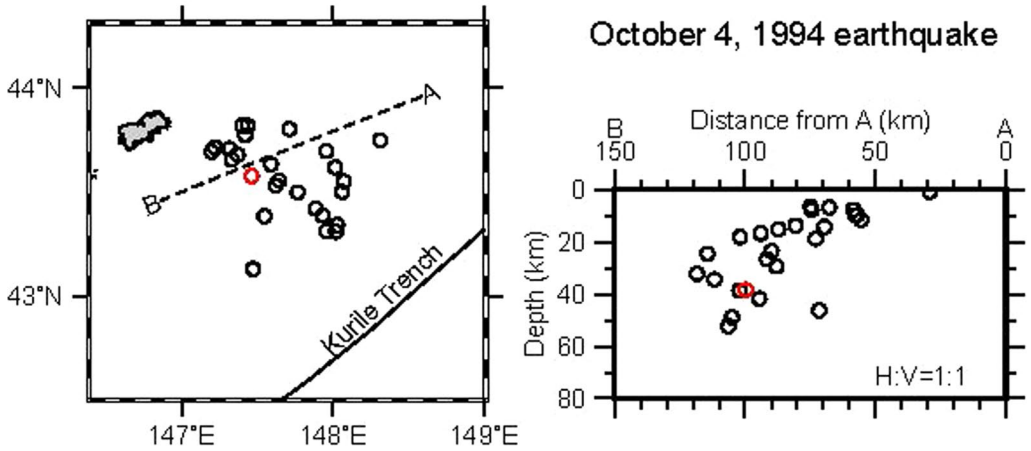

1 Introduction

The Pacific (PA) plate subducts beneath the North American (NA) plate from the Kurile Trench (KT) in the northwestern Pacific Ocean. The KT is an ocean trench extending from the east of the Kamchatka Peninsula to the southeast of Hokkaido along the southern coast of the Kurile Islands, with a length of 2200 km and an average width of 120 km. The PA plate moves toward N61° W at a speed of 82 mm/year relative to the NA plate (DeMets et al. 1994) off the east coast of Hokkaido, i.e., off Shikotan Island. This region is a study area of the present paper and referring as Hokkaido Toho-oki area.

Three earthquakes of different types occurred in the Hokkaido Toho-oki area (Fig. 1). The first is the August 11, 1969 Hokkaido Toho-oki earthquake (M_w8.2; U.S. Geological Survey 2024), a typical plate boundary megathrust earthquake; the second is the June 10, 1975 earthquake, which was a plate boundary megathrust earthquake like the 1969 event though it was not an ordinary earthquake but a tsunami earthquake (M_w7.8; Ioki and Tanioka 2016); the third is the October 4, 1994 Hokkaido Toho-oki earthquake (M_w8.3; U.S. Geological Survey 2024), an intraslab earthquake. Among the three earthquakes, the fault plane ruptured by the 1994 earthquake is still controversial issue, with some authors claiming that the strike is parallel to the KT axis (Kikuchi and Kanamori 1995; Katsumata et al. 1995; Hurukawa 1995; Ozawa 1996; Morikawa and Sasatani 2004), some authors claiming that it is almost perpendicular to the KT axis (Tanioka et al. 1995; Takahashi and Hirata 2003; Harada and Ishibashi 2007), and some authors claiming that it is unable to determine which is the fault plane (Tsuji et al. 1995).

In the case of the 1994 event, aftershocks determined by the Japanese seismic network, including Hokkaido University and Japan Meteorological Agency, appear to be along a fault plane parallel to the trench axis. Since the seismic stations are only in the west, the station coverage is poor geometrically. On the other hand, aftershocks determined by the global seismic network appear to be along a fault plane normal to the trench axis. Although the station coverage is better than the Japanese seismic

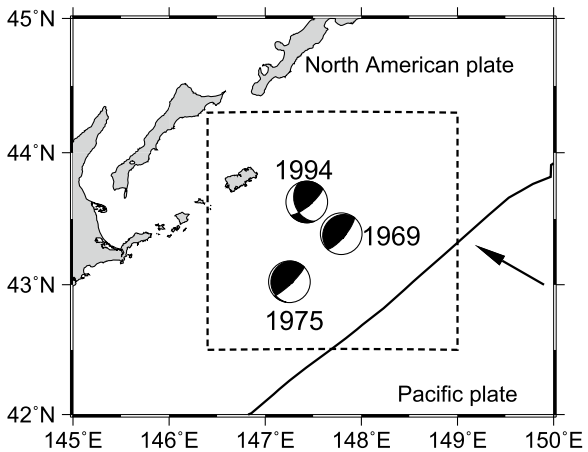

Fig. 1 The southwestern Kurile Islands area, which refer to as the Hokkaido Toho-oki area in the present study. Three earthquakes occurred in 1969, 1975 and 1994, and their epicenters and the focal mechanism solutions are plotted. A rectangle drawn by broken lines shows the area of map view of the following figures. A solid line in the ocean indicates the plate boundary between the Pacific plate and the North American plate (Bird 2003). An arrow points to the direction of the plate motion of the Pacific plate relative to the North American plate (DeMets et al. 1994)

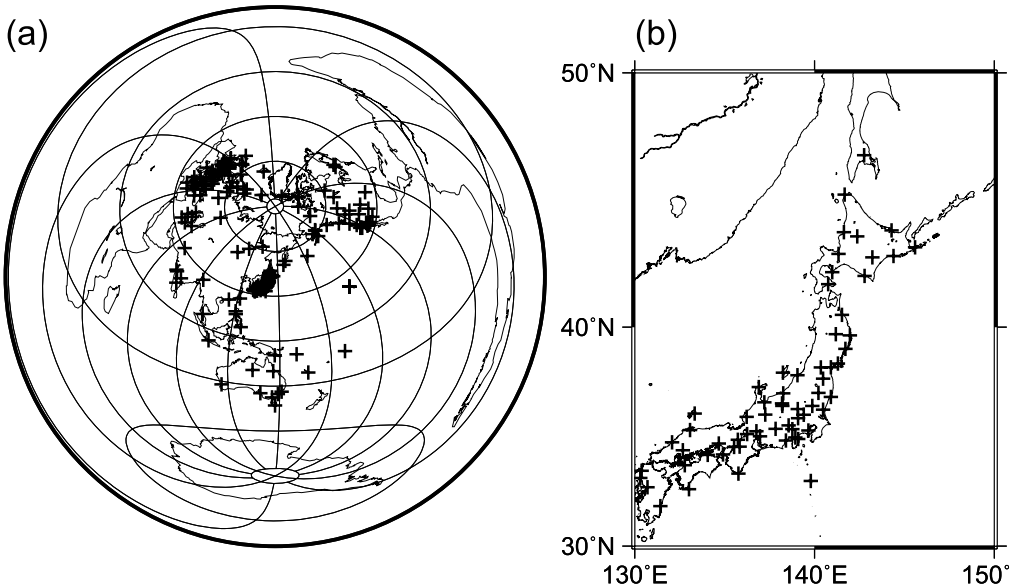

Fig. 2 Distribution of seismographic stations used for the hypocenter relocation. **a** All stations are plotted in crosses and **b** the enlarged view of the vicinity of Japan

network, the global seismic network is very far from the focal area. When the seismic stations are far away, the accuracy of depth determination is usually poor. Poor constraint of the aftershock determination is one of the reasons why the fault plane ruptured by the 1994 event has not been decided yet. In addition, the crustal deformation observed in Japan and the tsunami waveform are not conclusive evidence for determining the fault plane of the 1994 main shock because both fault planes can explain the observations to the same extent.

In this study, aftershock distributions of the 1994 event were re-determined and the source faults were examined based on the aftershock distribution. In addition, we calculate the Coulomb failure stress change (ΔCFS) due to the main shock and discuss which of the two nodal planes is more likely to trigger the largest aftershock. There are three points that differ from previous studies discussing the aftershock relocation of the 1994 event. First, the aftershocks of the 1969 and the 1975 events are also determined simultaneously with the 1994 event. The 1969 and 1975 earthquakes are known to have been interplate earthquakes, therefore, if their hypocenters are correctly determined, their aftershocks should be concentrated near the plate boundary. This will allow us to estimate whether the 1994 aftershocks were correctly determined. Second, I only used seismic stations that were already in existence at the time of the 1969 and 1975 earthquakes and that were also in existence at the time of the 1994 earthquake. In other words, I did not use seismic stations that were newly established or abolished after 1969. This reduces errors resulting from the difference of combinations of seismic stations. Third, the interaction between the main shock and the largest aftershock was examined in terms of static stress transfer.

2 Data

I downloaded the data from the *Reviewed ISC Bulletin* (https://download.isc.ac.uk/prerebuild/ffb/bulletin/). Hypocenter parameters and arrival times of the initial phase were used in this study. The initial phase is the seismic wave that arrived at a seismic station earliest, and it is usually P-wave. I did not re-measure the arrival time for myself by waveform correlation. I selected aftershocks with a body wave magnitude (m_b) equal to 5.3 or larger and a depth of less than 100 km for 7 days after the main shock. I selected 209 seismic stations that satisfy the following conditions: the epicentral distance from the Hokkaido Toho-oki area is smaller than 10,000 km and there are the P-wave arrival time data for all three earthquakes (Fig. 2). No S-wave arrival time was used. Consequently, the number of arrival time data is 6515 including the depth phase, i.e., 759 pP and 130 sP phases.

The arrival time data were weighted by the following equation (Waldhauser and Schaff 2007),

$$\mathrm{wt} = \left\{ \left(1 - \frac{\Delta}{130} \right)^3 \right\}^3$$

where wt is a weight factor and Δ is the epicentral distance in degree. For example, if $0° < \Delta \leq 48°$, wt = 0.9, if

$67° \leq \Delta \leq 73°$, wt = 0.6, and if $87° \leq \Delta \leq 93°$, wt = 0.3. In the weighting function, the interevent distance is replaced with the epicentral distance. Note that this is a different usage from Waldhauser and Schaff (2007) and the weight value is rounded to the second decimal place.

3 Methods

For hypocenter determination, I used a double-difference earthquake location method, HypoDD (Waldhauser and Ellsworth 2000). However, HypoDD calculates travel times assuming a horizontal layered velocity structure, but to use teleseismic P-waves, it is necessary to calculate travel times in a spherically stratified velocity structure of the Earth. In this study, I assumed a one-dimensional velocity structure *iasp91* and calculated travel times using the iaspei-tau package (Kennett and Engdahl 1991; Snoke 2009). The totaling 66 events were relocated, consisting of 25 aftershocks in 1969 including the main shock, 12 in 1975, and 29 in 1994. Approximately 21,000 datasets were created by taking the double-difference when the hypocentral distance was less than 50 km. For the inversion, the LSQR method was applied with a damping of 30.

The final hypocenter location and its error was estimated by the jack-knife method (Tichelaar and Ruff 1989). Half of the datasets was removed randomly and HypoDD was conducted to determine the hypocenters. This procedure was repeated 1000 times and I calculated the average position and the standard deviation σ of the 1000 scattered hypocenters. In the present study, the average position and $\pm 2\sigma$ were adopted as the final hypocenter location and its error, respectively.

All epicenters determined by ISC were assumed as the initial epicenter. The initial depth of hypocenter was assumed to be 10 km for the 1969 and the 1975 events. In the case of the 1994 events, the depth determined by ISC was mostly assumed as the initial value, but some aftershocks were moved slightly to avoid being an air focus. Consequently, the rms of the residual of P-wave was 2.36 s for the initial hypocenter location and decreased to 1.39 s (41% decrease) after two iterations of the LSQR.

4 Results

In the case of 1969 event, the epicenter of the main shock was located 73 km from the KT axis and the depth is 12 ± 3 km which is close to the upper surface of the subducting PA plate (Fig. 3). Comparing with the large slip area revealed by a tsunami waveform inversion (Ioki and Tanioka 2016), the hypocenter of the main shock, i.e., the rupture initiation point, is located at the shallow edge of the large slip area. Kikuchi and Fukao (1987) also found that the large subevent occurred in the deeper portion relative to the rupture initiation point. The aftershock area spans 140 km along the KT, i.e., 50 km long to the southwest from the epicenter and 90 km long to the northeast from the epicenter, and the width is 50 km. This aftershock distribution is consistent with the bilateral rupture propagation revealed by Kikuchi and Fukao (1987).

In the case of 1975 event, the epicenter of the main shock was located 71 km from the KT axis and the depth is 7 ± 1 km which is on the upper surface of the subducting PA plate (Fig. 4). The aftershock area spans 70 km northeastward from the epicenter along the KT and the width is 30 km, which is obviously narrower than the 1969 aftershock area. The 1969 and 1975 aftershock areas are not clearly separated, but the 1975 aftershocks appear to be concentrated around the shallow edge of the large slip area of the 1969 earthquake. Ioki and Tanioka (2016) found that the tsunami in 1975 was excited by the large slip near the KT axis. The 1975 aftershocks occurred not inside of this large slip area, but around the deep edge of it. This fact might suggest that the short-period seismic wave was radiated from the 1975 aftershock area, whereas, not radiated from the large slip area near the KT.

In the case of the 1994 event, the epicenter of aftershocks was located in the circular area with a diameter of $\sim$ 80 km and the hypocenter of the main shock was located at the depth of 38 ± 4 km, which is obviously deeper than those of the 1969 and the 1975 events (Fig. 5). The centroid moment tensor (CMT) solution was determined by the U. S. Geological Survey (2024) for the main shock as follows. The nodal plane 1 (np1) is represented by strike1 = 158°, dip1 = 34°, rake1 = 21°and the nodal plane 2 (np2) is represented by strike2 = 50°, dip2 = 78°, rake2 = 122°. The np2 is a plane with a steep dip and with a strike almost parallel to the KT axis, and the np1 is a plane with a shallow dip and with a strike almost perpendicular to the KT axis. To examine which plane, np1 or np2, the aftershocks occurred along, we created depth cross-sections corresponding to each plane. Although the aftershocks are not distributed exactly on the plane surface, they tend to become deeper toward the southwest and its dip angle is 30°–40°. This spatial pattern of aftershock distribution strongly suggests that the aftershocks occurred on the np1 and the np1 is a fault plane ruptured by the 1994 main shock. Almost all aftershocks are located deeper than the upper surface of the subducting PA plate and are included within the ruptured area with a co-seismic slip larger than 2 m. No aftershock occurs in the overriding NA plate except for the largest aftershock (M_w7.3; US Geological Survey 2024) on October 9, 1994. The epicenter of the largest aftershock is located around the northeastern edge of the aftershock area (Fig. 6). The depth of hypocenter is determined to be 2 ± 1 km in this

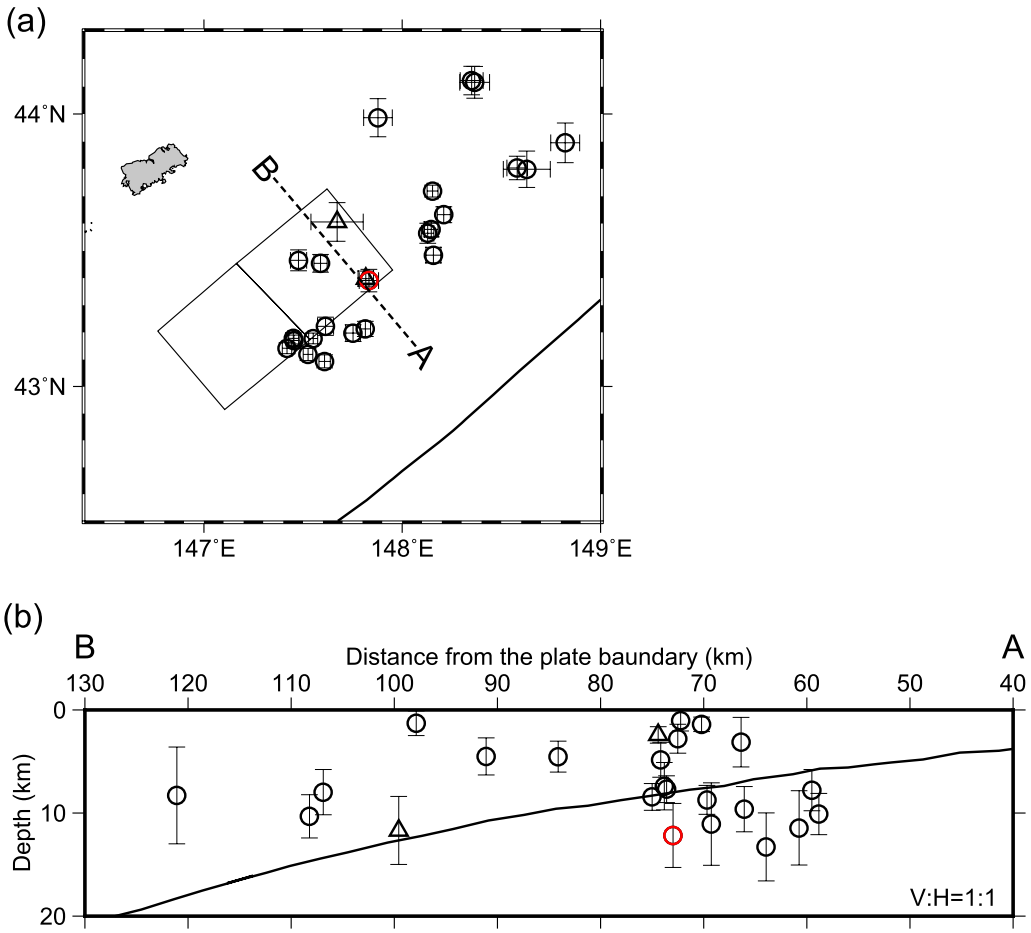

Fig. 3 The August 11, 1969 earthquake (M_W8.2) sequence with assuming the initial depth of 10 km for all 1969 events. **a** Epicenters distribution of the foreshocks (triangle), the main shock (red circle), and the aftershocks (black circle) after the relocation. A solid line in the ocean indicates the plate boundary between the Pacific plate and the North American plate (Bird 2003). Two squares indicate the subfaults 3 and 4 with large slip determined in Ioki and Tanioka (2016). **b** Vertical cross-sectional view along the broken line AB in **a**. A gently curved black line represents the upper boundary of the subducting Pacific plate (Nakanishi et al. 2004)

study and its depth is shallower significantly than the upper surface of the subducting PA plate. Only two aftershocks of the largest aftershock have been determined, but the depth is shallower than 5 km. This result implies that the largest aftershock occurred not within the subducting PA plate but within the upper crust of the landside NA plate.

5 Discussion

5.1 Hypocenter determination error

The accuracy of hypocenter determination is usually poor when using seismic stations far from the hypocenter. In particular, the depth of hypocenter is not likely to be well-constrained. In this section, we consider the possibility that the large depth error is the reason why the aftershocks do not show a planer distribution.

Since the hypocenter determination is a non-linear inversion, it is important how much hypocenter depth is assumed as the initial value. To check the effect of the initial hypocenter depth, I relocated hypocenters assuming that the initial depth of all aftershocks in 1994 is 40 km and the initial depth of all aftershocks in 1969 and 1975 is 10 km. This is a simpler assumption than assuming ISC depth for the 1994 event. The result is shown in Fig. S1 in Supplementary material 1. We found that the aftershock distribution is almost same regardless of the initial depth assumption.

To estimate the accuracy of depth determination, I conducted a numerical simulation as follows. First, 84 hypocenters were assumed to locate at nodes in three-dimensional space with 43.2, 43.3, and 43.4° N, 147.6, 147.8, 148.0, and 148.2° E, $h = 5$, 10, 15, 20, 25, 30, and 35 km in depth. Suppose that one of the 84 earthquakes is EQ1. The P-wave travel time for EQ1 was calculated using the Iaspei-tau package assuming a one-dimensional velocity structure iasp91. I randomly selected one of the

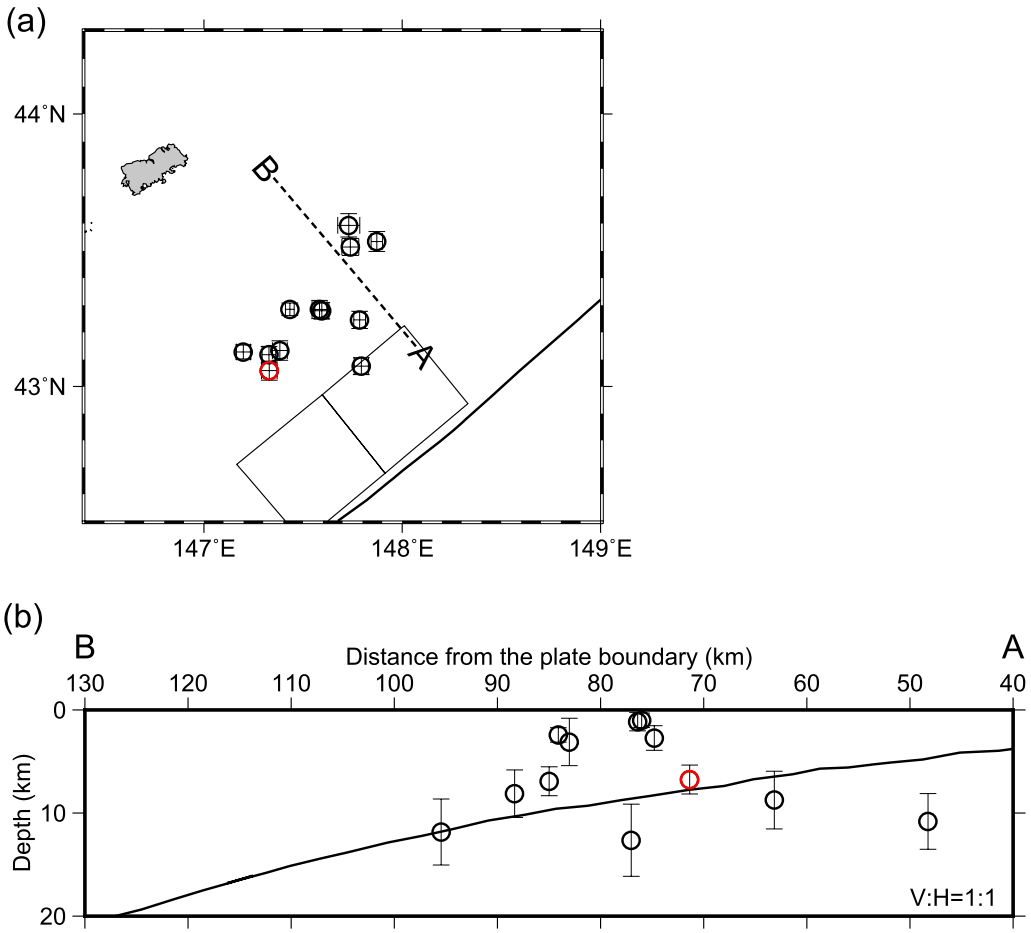

Fig. 4 The June 10, 1975 earthquake (M_w7.8) sequence with assuming the initial depth of 10 km for all 1975 events. **a** Epicenters distribution of the main shock (red circle) and the aftershocks (black circle) after the relocation. A solid line in the ocean indicates the plate boundary between the Pacific plate and the North American plate (Bird 2003). Two squares indicate the subfaults 6 and 7 with large slip determined in Ioki and Tanioka (2016). **b** Vertical cross-sectional view along the broken line AB in **a**. A gently curved black line represents the upper boundary of the subducting Pacific plate (Nakanishi et al. 2004)

66 earthquakes whose hypocenter was re-determined in this study and assumed that the combination of seismic stations for EQ1 was the same combination of seismic stations as the selected earthquake. Like EQ1, seismic stations were assigned to the 84 earthquakes and the theoretical travel time of P-waves was calculated. Random noise was not added to the travel time of P-waves. Using this data, I set the same parameters, e.g., damping, maximum distance of linked pair, iteration times, as in the actual calculation and determined the hypocenter using HypoDD. As the initial values for the epicenter, the assumed epicenter was given as is, and the depth was randomly assumed within the range of $h \pm 10$ km. The above procedure was repeated 500 times to evaluate how accurately the depth of hypocenter could be determined.

As a result of the numerical simulation, we found that the depth of hypocenter tends to be determined deeper than the true location (Fig. 7). If the true depth of hypocenter is 0–5 km, there will be a shift of 0–7 km toward the deeper side. If the true depth is 30–35 km, there will be a shift of 2–10 km toward the deeper side. This result suggests that the initial value is important, if the initial epicenter is assumed to be close to the true epicenter and the initial depth is assumed to be ± 10 km from the true depth, the error of depth will be approximately several kilometers. As a result, the hypocenter may appear to scatter over a range of several kilometers in the depth direction. In the case of the 1994 event, this may be a reason why the aftershocks are scattered in depth direction and not distributed on a plane clearly.

5.2 Coulomb failure stress change on the largest aftershock source fault

It is clearly shown from the aftershock distribution relocated in the present study that the 1969 and the 1975 events are interplate megathrust earthquakes and the

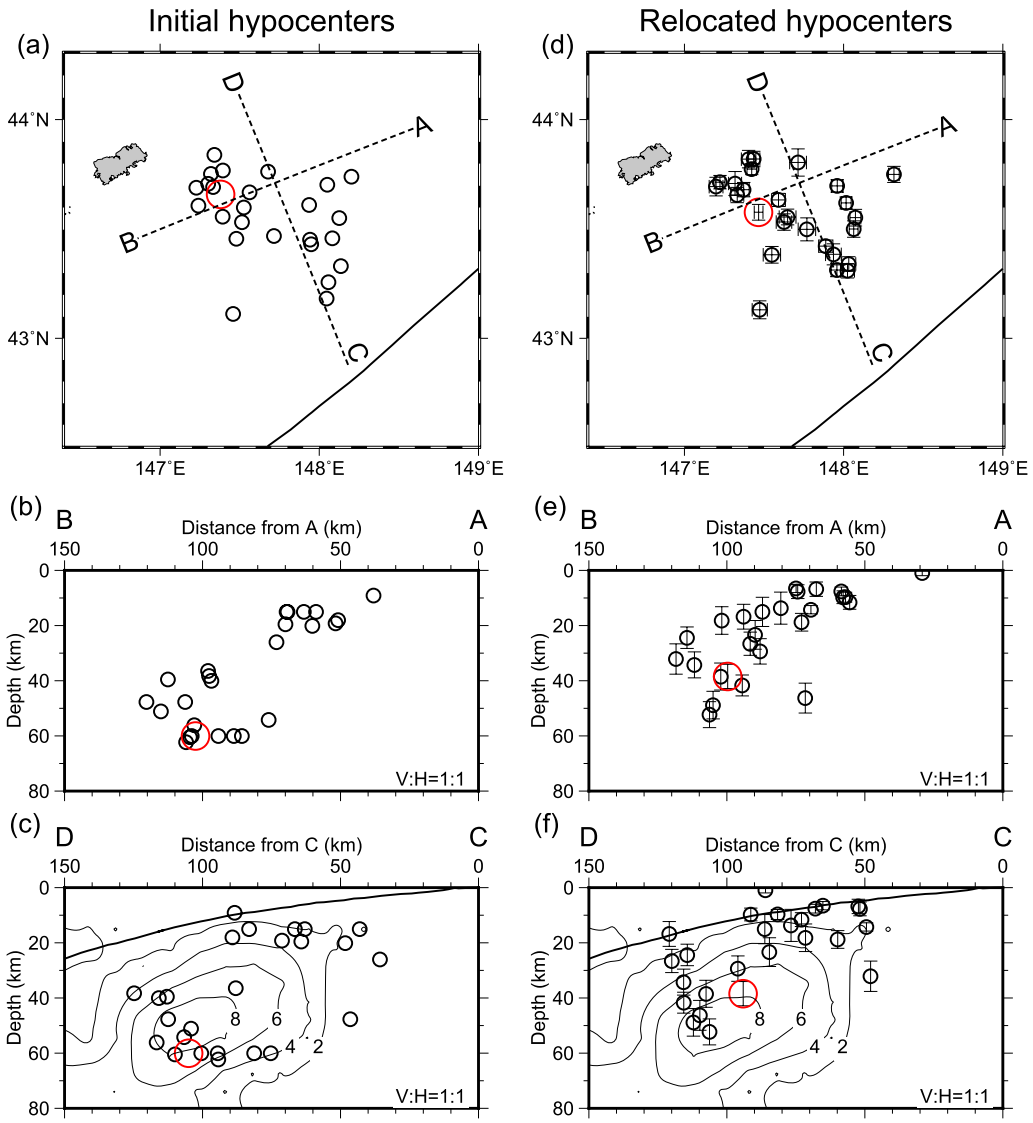

Fig. 5 The October 4, 1994 earthquake (M_w8.3) sequence. **a**–**c** The initial value of hypocenters before the relocation, and **d**–**f** are the hypocenters after the relocation. **a**, **d** Epicenters distribution of the main shock (red circle) and the aftershocks (black circle) before the relocation. A solid line in the ocean indicates the plate boundary between the Pacific plate and the North American plate (Bird 2003). **b**, **e** Vertical cross-sectional view along the broken line AB. **c**, **f** Vertical cross-sectional view along the broken line CD. A gently curved black line represents the upper boundary of the subducting Pacific plate (Nakanishi et al. 2004). Contours of 2, 4, 6, and 8 m show the co-seismic slip distribution (U.S. Geological Survey 2024)

1994 event is not interplate but intraslab earthquake. Moreover, it is preferable that the strike of the 1994 source fault is not parallel but perpendicular to the KT axis. To examine the geometry of the 1994 event from a different perspective, we calculate ΔCFS to investigate which fault plane is more favorable for the occurrence of the largest aftershock.

Tanioka et al. (1995) suggested qualitatively that some aftershocks were triggered in the area northeast of the 1994 source fault. To confirm this hypothesis quantitatively, I calculate ΔCFS on the fault plane of the largest aftershock. Tsuji et al. (1995) presented the main shock fault models: Model 1 which is parallel to the KT axis and Model 2 which is perpendicular to the KT axis. As for the fault parameters of Models 1 and 2, the values shown in Table 2 of Tsuji et al. (1995) were assumed. The source fault of the M_w7.3 largest aftershock is assumed to be a rectangle with a length of 30 km and a width of 15 km. The top of the rectangular fault was assumed to be 0 km deep. The CMT solution of the largest aftershock was provided by the U.S. Geological Survey (2024) as follows. The nodal plane 1 (NP1) is represented by strike = 219°,

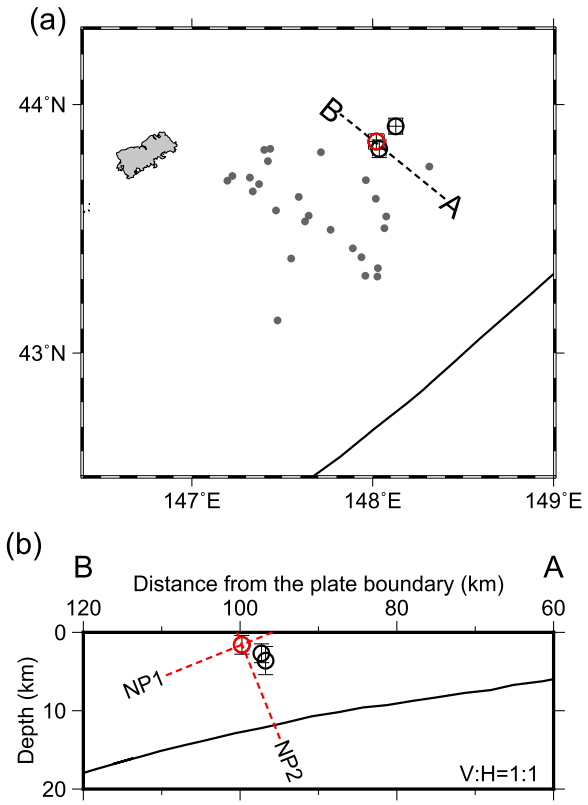

Fig. 6 The October 9, 1994 largest aftershock (M_w7.3) sequence. **a** Epicenters distribution of the main shock of the largest aftershock (red circle) and its secondary aftershocks (black circle) after the relocation. Gray dots show the epicenters plotted in Fig. 5d. A solid line in the ocean indicates the plate boundary between the Pacific plate and the North American plate (Bird 2003). **b** Vertical cross-sectional view along the broken line AB in **a**. NP1 and NP2 indicate two nodal planes of the largest aftershock. A gently curved black line represents the upper boundary of the subducting Pacific plate (Nakanishi et al. 2004)

dip = 22°, rake = 90° and the nodal plane 2 (NP2) is represented by strike = 39°, dip = 68°, rake = 90°. The 30 km long fault was placed so that the epicenter relocated in this study matches with a center of the fault (Fig. 6b).

The ΔCFS caused by the source faulting, i.e., Models 1 and 2, were calculated on the receiver's fault plane, i.e., NP1 and NP2 (Fig. 8). The ΔCFS is defined by $\Delta CFS = \Delta\tau + \mu\Delta\sigma$, where $\Delta\tau$ is the shear stress change on a fault and $\Delta\sigma$ is the normal stress change. μ is the effective friction coefficient (with a range of 0–1). Failure is encouraged if ΔCFS is positive and discouraged if negative (e.g., Stein and Lisowski 1983; Stein 1999). $\Delta\tau$ and $\Delta\sigma$ are calculated in an elastic half-space based on Okada (1992) assuming that the shear modulus is 3.0×10^{10} N/m^2 and the Poisson's ratio is 0.25. The effective friction coefficient is taken to be 0.4.

As a result, we found that ΔCFS is negative on both receiver's faults if Model 1 is assumed for the source fault and ΔCFS is positive on both receiver's faults if Model 2 is assumed. The average ΔCFS on NP1 is −0.020 MPa for Model 1 and +0.088 MPa for Model 2. The average ΔCFS on NP2 is −0.020 MPa for Model 1 and +0.076 MPa for Model 2. Regardless of the fault plane of the largest aftershock, Model 2 results in a positive ΔCFS, suggesting that the main shock rupture represented by Model 2 is more likely to trigger the largest aftershock than Model 1. The value of ∼ 0.08 MPa is several times larger than the threshold of triggering, i.e., 0.01 MPa (Stein 1999).

5.3 Possible causes of the 1994 Hokkaido Toho-oki earthquake

The cause of earthquakes varies depending on which is considered the fault plane of the 1994 event. In the case of the trench-parallel fault plane, the main shock was caused primarily by the down-dip extensional stress within the subducting PA plate. Although there is a small right-lateral strike-slip component, the movement is mainly normal faulting within the PA plate. In the case of trench-normal fault plane, the main shock was caused primarily by the compressional stress in the direction of NW–SE, and the faulting was mainly characterized by left-lateral strike-slip motion with a small reverse fault component. The NW–SE compressional stress might be due to the oblique subduction of the PA plate and the southwestern movement of the forearc sliver of the Kurile

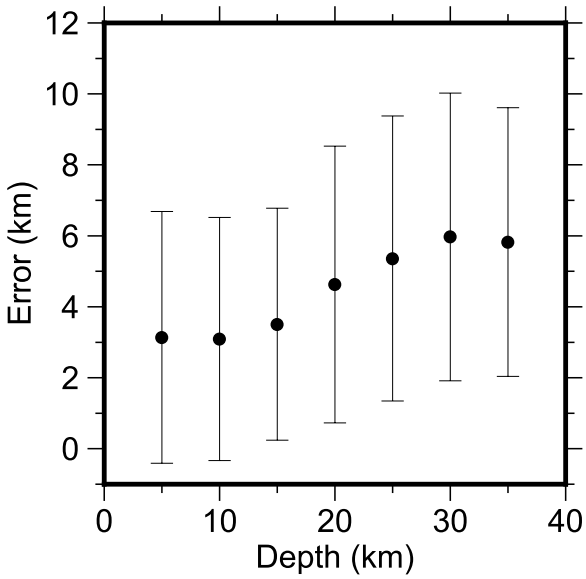

Fig. 7 Hypocenter determination error in depth direction estimated by a numerical simulation. The error is defined as a shift from the assumed true location. I collected the errors for hypocenters at the same depth and calculated the mean and variance for each depth

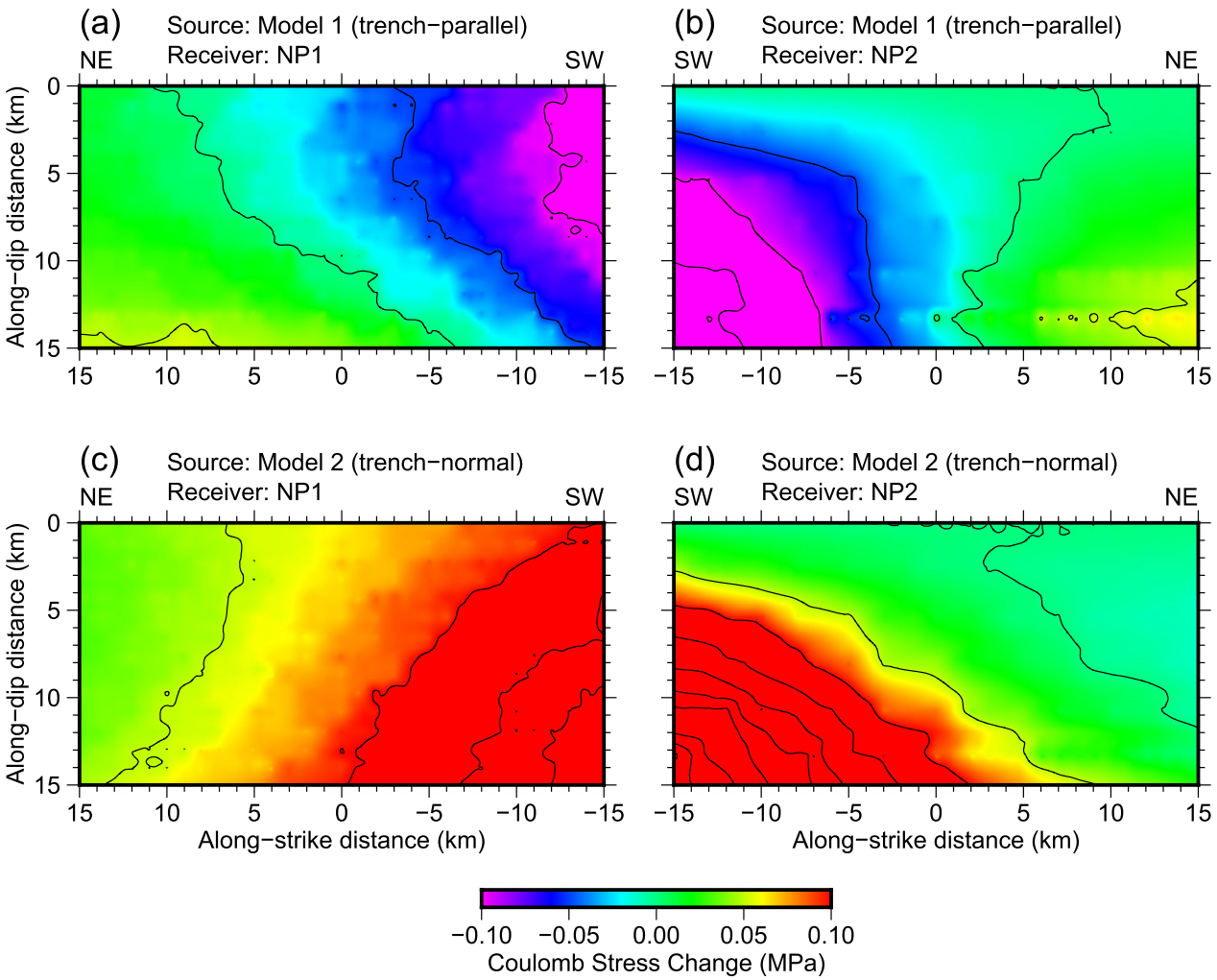

Fig. 8 Coulomb stress change on the nodal planes of the largest aftershock associated with the 1994 event. The fault ruptured by the main shock is assumed based on the model presented on Table 2 of Tsuji et al. (1995). Model1 and Model2 are referred as Trench-parallel model and Trench-normal model, respectively. The nodal planes of the largest aftershock are represented as follows: NP1 (strike = 219°, dip = 22°, rake = 90°) and NP2 (strike = 39°, dip = 68°, rake = 90°) (U.S. Geological Survey 2024). **a** Shows the case that the fault plane of the main shock is assumed to be Trench-parallel model and the fault plane of the largest aftershock is assumed to be NP1, **b** trench-parallel and NP2, **c** trench-normal and NP1, **d** trench-normal and NP2. Contours are drawn every 0.05 MPa

Islands also driven by the oblique subduction (DeMets 1992). As pointed out by Tanioka et al. (1995), since here is a fracture zone, the strain may be more likely to concentrate.

6 Conclusion

In the Hokkaido Toho-oki area, that is, off Shikotan Island, three large earthquakes occurred in 1969, 1975, and 1994. In this study, the relative location of aftershocks of the three earthquakes were determined simultaneously using HypoDD. As a result, the aftershocks of the 1969 and 1975 events were located near the upper surface of the subducting PA plate suggesting that these two events are interplate megathrust earthquakes. On the other hand, the aftershocks of the 1994 event were not concentrated near the upper surface of the PA plate, but distributed within the PA plate, suggesting that the 1994 event is an intraslab event. Moreover, the aftershock distribution tends to become deeper toward the southwest and its dip angle is 30°–40°. Even if taking the hypocenter location error into account, the aftershocks are distributed along a fault plane perpendicular to the KT axis. The calculation of ΔCFS showed that the trench-normal fault plane is more efficient at triggering the largest aftershock. Not only the aftershock distribution but also ΔCFS

supported the trench-normal fault plane of the 1994 main shock.

Supplementary Information

The online version contains supplementary material available at https://doi.org/10.1186/s40623-024-02069-6.

Additional file1

Acknowledgements
The thoughtful comments from an editor, Bogdan Enescu, and the anonymous reviewers were extremely helpful in revising the manuscript. GMT-SYSTEM (Wessel and Smith 1991) was used for mapping data. MICAP-G (Naito and Yoshikawa 1999) was used to calculate changes in the Coulomb failure stress.

Author contributions
KK was a major contributor in analyzing data and writing the manuscript.

Funding
This study was partly supported by the Ministry of Education, Culture, Sports, Science and Technology (MEXT) of Japan, under its "The Second Earthquake and Volcano Hazards Observation and Research Program (Earthquake and Volcano Hazard Reduction Research)".

Availability of data and materials
The datasets used and/or analyzed during the current study are available from the corresponding author on reasonable request.

Declarations

Competing interests
The authors declare that they have no competing interests.

Author details
[1]Institute of Seismology and Volcanology, Faculty of Science, Hokkaido University, Sapporo 060-0810, Japan.

Received: 14 April 2024 Accepted: 16 September 2024
Published online: 29 September 2024

References

Bird P (2003) An updated digital model of plate boundaries. Geochem Geophys Geosyst 4(3):1027. https://doi.org/10.1029/2001GC000252
DeMets C (1992) Oblique convergence and deformation along the Kuril and Japan Trenches. J Geophys Res 97:17615–17625. https://doi.org/10.1029/92JB01306
DeMets C, Gordon RG, Argus DF, Stein S (1994) Effect of recent revisions to the geomagnetic reversal time scale on estimates of current plate motions. Geophys Res Lett 21:2191–2194. https://doi.org/10.1029/94GL02118
Harada T, Ishibashi K (2007) Two parallel trench-normal fault planes within the Pacific slab associated with the 1994 and 2000 Kurile earthquakes as revealed by simultaneous relocation of their main shocks and aftershocks. Earth Planets Sp 59:e25–e28. https://doi.org/10.1186/BF03352025
Hurukawa N (1995) Quick relocation of the 1994 Shikotan earthquake and its fault planes. Geophys Res Lett 22(23):3159–3162. https://doi.org/10.1029/95GL03167
Ioki K, Tanioka Y (2016) Rupture process of the 1969 and 1975 Kurile earthquakes estimated from tsunami waveform analyses. Pure Appl Geophys 173:4179–4187. https://doi.org/10.1007/s00024-016-1402-0
Katsumata K, Ichiyanagi M, Miwa M, Kasahara M, Miyamachi H (1995) Aftershock distribution of the October 4, 1994 Mw8.3 Kurile Islands earthquake determined by a local seismic network in Hokkaido, Japan. Geophys Res Lett 22(11):1321–1324. https://doi.org/10.1029/95GL01316
Kennett BLN, Engdahl ER (1991) Traveltimes for global earthquake location and phase identification. Geophys J Int 105(2):429–465. https://doi.org/10.1111/j.1365-246X.1991.tb06724.x
Kikuchi M, Fukao Y (1987) Inversion of long-period P-waves from great earthquakes along subduction zones. Tectonophysics 144:231–247. https://doi.org/10.1016/0040-1951(87)90020-5
Kikuchi M, Kanamori H (1995) The Shikotan earthquake of October 4, 1994: lithospheric earthquake. Geophys Res Lett 22(9):1025–1028. https://doi.org/10.1029/95GL00883
Morikawa N, Sasatani T (2004) Source models of two large intraslab earthquakes from broadband strong ground motions. Bull Seismol Soc Am 94(3):803–817. https://doi.org/10.1785/0120030033
Naito H, Yoshikawa S (1999) A program to assist crustal deformation analysis [in Japanese with English figure captions]. J Seismol Soc Jpn 52:101–103. https://doi.org/10.4294/zisin1948.52.1_101
Nakanishi A, Smith AJ, Miura S, Tsuru T, Kodaira S, Obana K, Takahashi N, Cummins PR, Kaneda Y (2004) Structural factors controlling the coseismic rupture zone of the 1973 Nemuro-Oki earthquake, the southern Kuril Trench seismogeniczone. J Geophys Res 109:B05305. https://doi.org/10.1029/2003JB002574
Okada Y (1992) Internal deformation due to shear and tensile faults in a half-space. Bull Seismol Soc Am 82(2):1018–1040. https://doi.org/10.1785/BSSA0820021018
Ozawa S (1996) Geodetic inversion for the fault model of the 1994 Shikotan earthquake. Geophys Res Lett 23(16):2009–2012. https://doi.org/10.1029/96GL02049
Snoke JA (2009) Traveltime tables for *iasp91* and *ak135*. Seismol Res Lett 80(2):260–262. https://doi.org/10.1785/gssrl.80.2.260
Stein RS (1999) The role of stress transfer in earthquake occurrence. Nature 402:605–609. https://doi.org/10.1038/45144
Stein RS, Lisowski M (1983) The 1979 Homestead Valley earthquake sequence, California: control of aftershocks and postseismic deformation. J Geophys Res 88(8):6477–6490. https://doi.org/10.1029/JB088iB08p06477
Takahashi H, Hirata K (2003) The 2000 Nemuro-Hanto-Oki earthquake, off eastern Hokkaido, Japan, and the high intraslab seismic activity in the southwestern Kuril Trench. J Geophys Res 108(B4):2178. https://doi.org/10.1029/2002JB001813
Tanioka Y, Ruff L, Satake K (1995) The great Kurile earthquake of October 4, 1994 tore the slab. Geophys Res Lett 22(13):1661–1664. https://doi.org/10.1029/95GL01656
Tichelaar BW, Ruff LJ (1989) How good are our best models? Jackknifing, bootstrapping, and earthquake depth. Eos 70(20):593–606. https://doi.org/10.1029/89EO00156
Tsuji H, Hatanaka Y, Sagiya T, Hashimoto M (1995) Coseismic crustal deformation from the 1994 Hokkaido-Toho-Oki earthquake monitored by a nationwide continuous GPS array in Japan. Geophys Res Lett 22(13):1669–1672. https://doi.org/10.1029/95GL01659
U. S. Geological Survey (2024) Search Earthquake Catalog accessed March 18, 2024 at URL https://earthquake.usgs.gov/earthquakes/search/
Waldhauser F, Ellsworth WL (2000) A double-difference earthquake location algorithm: method and application to the northern Hayward fault, California. Bull Seismol Soc Am 90(6):1353–1368. https://doi.org/10.1785/0120000006
Waldhauser F, Schaff D (2007) Regional and teleseismic double-difference earthquake relocation using waveform cross-correlation and global bulletin data. J Geophys Res 112:B12301. https://doi.org/10.1029/2007JB004938
Wessel P, Smith WHF (1991) Free software helps map and display data. Eos Trans AGU 72:445–446. https://doi.org/10.1029/90EO00319

Publisher's Note